

# 元素掺杂 DLC 薄膜在模拟油气田溶液中的耐蚀与耐磨性

刘政宇<sup>1,2</sup>, 丛浩宇<sup>3</sup>, 牟成龙<sup>1,2</sup>, 曹学乾<sup>1\*</sup>, 张广安<sup>1,2\*</sup>, 薛群基<sup>1</sup>

(1.中国科学院兰州化学物理研究所, 兰州 730000; 2.中国科学院大学, 北京 100049;

3.山东大学 机电与信息工程学院, 山东 威海 264209)

**摘要:** **目的** 沉积出在含有泥沙的模拟油气田溶液中具有优异耐蚀性与耐磨性的类金刚石碳基 (DLC) 薄膜来对油气开采时的管道进行保护。**方法** 通过等离子体增强化学气相沉积 (PECVD) 技术在 SS304 方形试样表面沉积 H-DLC、F-HDLC、N-HDLC 及 Si-HDLC, 通过电化学测试表征了其在模拟油气田 CO<sub>2</sub>/H<sub>2</sub>S/Cl<sup>-</sup> 溶液中的耐蚀性。采用 CSM 往复摩擦试验机测试了其在含有泥沙的模拟溶液中的耐蚀性, 结合拉曼光谱、扫描电镜 (SEM) 等技术分析了摩擦测试后的磨斑与磨痕形貌。**结果** DLC 薄膜的沉积显著提高了 SS304 基底的耐蚀性, Si 掺杂的 DLC 薄膜具有最高的孔隙电阻与最低的腐蚀电流密度, 沉积薄膜后的腐蚀电流密度与 SS304 基底相比降低了 2 个数量级。沉积 DLC 薄膜后 SS304 基底的耐磨性大幅提高, 转移膜的形成降低了摩擦因数与磨损率, 薄膜的沉积使磨损率降低了约 2 个数量级, 在与模拟沙粒的 SiO<sub>2</sub> 对偶球进行摩擦时转移膜仍能稳定形成。通过向腐蚀溶液中添加 SiO<sub>2</sub> 粉末模拟了 SS304 基底与 DLC 薄膜在含有大量泥沙的油气采出水中的磨损, 摩擦测试后 SS304 基底表面发生严重的磨粒磨损, 不同元素掺杂的 DLC 薄膜表面均存在不同程度的剥落, 但与基底相比极大地缓解了基底磨损。**结论** DLC 薄膜的沉积可以极大地提高 SS304 基底的耐蚀性与耐磨性, Si-HDLC 薄膜在模拟油气田溶液中具有最优越的耐蚀性与稳定性, 进而使其在腐蚀溶液中具有优异的耐磨性。

**关键词:** 油气田; 管道保护; DLC; 耐蚀性; 耐磨性; 泥沙磨损

中图分类号: TH117; TG174 文献标志码: A 文章编号: 1001-3660(2024)11-0035-10

DOI: 10.16490/j.cnki.issn.1001-3660.2024.11.003

## Corrosion Resistance and Wear Resistance of Element Doped DLC Films in Simulated Oil and Gas Field Solution

LIU Zhengyu<sup>1,2</sup>, CONG Haoyu<sup>3</sup>, MOU Chenglong<sup>1,2</sup>, CAO Xueqian<sup>1\*</sup>,  
ZHANG Guang'an<sup>1,2\*</sup>, XUE Qunji<sup>1</sup>

(1. Lanzhou Institute of Chemical Physics, Chinese Academy of Sciences, Lanzhou 730000, China;

2. University of Chinese Academy of Sciences, Beijing 100049, China;

3. School of Mechanical, Electrical & Information Engineering, Shandong University, Shandong Weihai 264209, China)

收稿日期: 2024-04-01; 修订日期: 2024-05-31

Received: 2024-04-01; Revised: 2024-05-31

基金项目: 国家自然科学基金区域创新发展联合基金 (U21A20127); 国家自然科学基金面上项目 (52275221)

Fund: Joint Funds of the National Natural Science Foundation of China (U21A20127); National Natural Science Foundation of China (52275221)

引文格式: 刘政宇, 丛浩宇, 牟成龙, 等. 元素掺杂 DLC 薄膜在模拟油气田溶液中的耐蚀与耐磨性[J]. 表面技术, 2024, 53(11): 35-44.

LIU Zhengyu, CONG Haoyu, MOU Chenglong, et al. Corrosion Resistance and Wear Resistance of Element Doped DLC Films in Simulated Oil and Gas Field Solution[J]. Surface Technology, 2024, 53(11): 35-44.

\*通信作者 (Corresponding author)

**ABSTRACT:** Oil and gas resources are the main energy and chemical raw materials in the world today. Under the premise of limited total reserves of oil and gas resources, in order to improve the efficiency of oil and gas exploitation, CO<sub>2</sub> flooding technology is widely used. However, CO<sub>2</sub> flooding technology aggravates the acidification of oilfield produced water, so that oil and gas production pipelines are in a solution containing CO<sub>2</sub>/H<sub>2</sub>S/Cl<sup>-</sup> for a long time. The oilfield produced water solution has strong permeability and corrosivity. At the same time, the oil and gas exploitation is also faced with the abrasion of sand, which aggravates the corrosion. Therefore, there is an urgent need for a material to protect the inner surface of oil and gas exploitation pipelines. At present, the methods of protecting oil and gas exploitation pipelines have the defects of environmental pollution and high cost. At the same time, it is difficult to protect pipelines in the harsh environment of oil and gas exploitation. Diamond-like carbon (DLC) film with high hardness, high wear resistance and high corrosion resistance is an excellent protective material for oil and gas pipelines. In this work, H-DLC, F-HDLC, N-HDLC and Si-HDLC were deposited on the surface of SS304 square sample by plasma enhanced chemical vapor deposition (PECVD) technology, and their corrosion resistance in CO<sub>2</sub>/H<sub>2</sub>S/Cl<sup>-</sup> solution of simulated oil and gas fields was characterized by electrochemical test. The CSM reciprocating friction machine was used to test the corrosion resistance in simulated solution containing sediment. The wear scar and its morphology after friction test were analyzed by Raman spectroscopy and scanning electron microscopy (SEM). The deposition of DLC film significantly improved the corrosion resistance of SS304 substrate. The doping of Si element reduced the internal stress of DLC film, and increased the content of sp<sup>3</sup>-C hybridization, and greatly improved the corrosion resistance of H-DLC film. The Si-doped DLC film possessed the highest pore resistance and the lowest corrosion current density, and had the best corrosion resistance in simulated oil and gas field solution. The wear resistance of SS304 substrate was greatly improved after deposition of DLC film. The formation of transfer film reduced the friction coefficient and wear rate. The transfer film could still be formed stably when rubbing with the SiO<sub>2</sub> counterpart ball of simulated sand. The wear of SS304 substrate and DLC film in oil and gas produced water containing a large amount of sediment was simulated by adding SiO<sub>2</sub> powder to the corrosion solution. After the friction test, severe abrasive wear occurred on the surface of SS304 substrate. The surface of DLC film doped with different elements had different degrees of spalling, but it greatly alleviated the wear of the substrate compared with the substrate. The deposition of DLC film can greatly improve the corrosion resistance and wear resistance of SS304 substrate. Si-HDLC film possesses the best corrosion resistance and stability in simulated oil and gas field solution, which makes it have excellent wear resistance in corrosion solution.

**KEY WORDS:** oil and gas fields; pipeline protection; DLC; corrosion resistance; wear resistance; sand abrasion

在油气资源总储量有限的前提下, CO<sub>2</sub> 驱油技术是提高油气生产效率的有效策略<sup>[1-2]</sup>。CO<sub>2</sub> 驱油技术加剧了油田采出水的酸化, 使油气开采管道长期处于含有 CO<sub>2</sub>/H<sub>2</sub>S/Cl<sup>-</sup> 的溶液中<sup>[3-4]</sup>。油田采出水中的腐蚀性离子具有极强的渗透性, 加速了管道的点蚀与硫化物应力开裂的发生<sup>[5-6]</sup>。同时油气开采时还存在着泥沙导致的磨损, 泥沙与腐蚀溶液一起导致油气开采时管道内表面的损伤, 造成重大的经济损失和安全风险<sup>[7-9]</sup>。

通过表面改性在金属表面引入保护膜的方法能有效解决上述问题, 然而喷涂和电镀等传统减缓油气开采管道腐蚀的保护膜带来了严重的环境污染, 而且不足以应对恶劣的腐蚀环境<sup>[10]</sup>。类金刚石碳基(DLC)薄膜具有高硬度、高耐磨性及高耐蚀性, 是一种优异的油气管道保护材料, 将异质非金属元素结合到本征 DLC 结构中可以进一步提高其耐蚀性<sup>[11-14]</sup>, N 元素掺杂能提高 DLC 薄膜的韧性和黏合强度, 从而防止腐蚀过程中裂纹的扩展<sup>[15-16]</sup>, F 元素的掺杂能提高 DLC 薄膜的疏水性<sup>[17-18]</sup>, Si 元素的掺杂能够形成绝缘氧化硅(SiO<sub>x</sub>)来提高薄膜致密性<sup>[19]</sup>, 这 3 种元素的掺杂

有望提高 DLC 薄膜在模拟油气开采环境中的耐蚀性与耐磨性。目前, Si-DLC 薄膜在模拟油气田环境中的优异耐蚀性已经得到了证实, Si-DLC 薄膜在温度变化及 H<sub>2</sub>S 浓度变化的腐蚀环境中仍具有良好的稳定性<sup>[20]</sup>。然而, 油气田环境中还存在着泥沙磨损导致的磨蚀, Si 元素及其余非金属元素的掺杂对其在模拟油气田环境中的耐蚀与耐磨性影响仍缺乏相关研究。

本文通过等离子体增强化学气相沉积技术在 SS304 方形试样上沉积了 H-DLC、F-HDLC、N-HDLC 及 Si-HDLC 4 种元素掺杂的 DLC 薄膜。将电化学测试、摩擦试验宏观分析技术、拉曼光谱和 SEM 等形貌结构表征技术相结合, 研究了 4 种元素掺杂 DLC 薄膜在模拟油气田溶液中的耐蚀性与耐磨性。

## 1 试验

### 1.1 涂层制备

以 304 不锈钢(SS304)方形试样(30 mm×

30 mm×2 mm) 作为基底, 将样品依次浸入石油醚、丙酮和酒精溶液中超声清洗以去除样品表面的油污, 清洁后的样品被置于腔体内的样品架上并连接电源阴极, 通过机械泵和分子泵使腔体处于高真空状态 ( $3\times10^{-3}$  Pa), 后续通过干泵抽气使 DLC 薄膜在沉积过程中保持恒定压力。薄膜的具体沉积工艺如下:

首先通入氩气并对样品施加负偏压, 通过产生的高密度氩等离子体对基底表面进行刻蚀以清洁样品表面; 接着同时引入氩气和硅烷气体, 在负偏压的作用下沉积 Si 过渡层来增强基底与 DLC 薄膜之间的结合力; 最后通过表 1 中的沉积参数在 SS304 表面分别沉积 H-DLC、F-HDLC、N-HDLC 和 Si-HDLC。

表 1 不同元素掺杂 DLC 薄膜的沉积参数  
Tab.1 Deposition parameters of DLC films doped with different elements

Sample	Gas precursor					Pressure/Pa	Voltage/kV	Time/min
	Ar	CF <sub>4</sub>	N <sub>2</sub>	SiH <sub>4</sub>	C <sub>2</sub> H <sub>2</sub>			
H-DLC	100	—	—	—	150	7.5	0.8	40
F-HDLC	100	50	—	—	150	7.5	0.8	40
N-HDLC	100	—	50	—	150	7.5	0.8	40
Si-HDLC	100	—	—	50	150	7.5	0.8	40

1.2 薄膜性能表征

1) 使用激发波长为 532 nm 的 LabRAM HR Evolution 共焦显微镜来获得拉曼光谱, 通过场发射电子显微镜 (FESEM, TESCAN, MIRA3) 对薄膜的横截面及摩擦测试后的磨痕和磨斑进行了测试。使用纳米压痕测试仪 (Anton Paar, TTXNHT2) 评估了不同元素掺杂 DLC 薄膜的弹性模量与硬度, 试验中使用的压头是 Berkovich 圆锥形金刚石压头, 圆锥形的顶角为  $65.3^{\circ}\pm0.3^{\circ}$ , 与衬底接触部分的宽度为 2  $\mu\text{m}$ , 试验过程中施加的压痕速度为 6 mN/min。采用划痕仪 (RST3, Anton Paar) 测试薄膜结合力, 划痕初始负载为 0.5 N, 最终负载为 20 N, 划痕长度为 3 mm。

2) 使用电化学工作站 (Autolab, PGSTAT302N) 测量了 DLC 薄膜的动电位极化曲线与电化学阻抗谱。测试的溶液为模拟 CO<sub>2</sub>-H<sub>2</sub>S-Cl<sup>-</sup>溶液, 向质量分数为 3.5% 的 NaCl 溶液中依次通入 1 h 氮气和 CO<sub>2</sub> 气体获得 CO<sub>2</sub> 饱和 NaCl 溶液, 向溶液中加入质量分数为 1.2% 的 Na<sub>2</sub>S·9H<sub>2</sub>O 并调节溶液 pH 值为 4 来模拟含有 H<sub>2</sub>S 的溶液环境。电化学测试中的工作电极为 4 种不同元素掺杂的 DLC 薄膜, 参比电极和对电极分别为饱和甘汞电极和铂电极, 在测试前将样品置于溶液中 30 min 以获得稳定的开路电位, 薄膜与腐蚀溶液间接接触的面积为 0.13 cm<sup>2</sup>, 动电位极化曲线测试是以 10 mV/s 的扫描速度从 -1 V (vs. Ref) 扫描至 0.8 V (vs. Ref)。EIS 测量的频率为 10<sup>5</sup>~10<sup>-2</sup> Hz, 振幅为 10 mV。

3) 使用往复式 CSM 摩擦机 (TRN 0204015, 瑞士) 对不同元素掺杂 DLC 薄膜和 SS304 基底的摩擦学性能进行测试。为了模拟油气田中沙粒的磨损, 摩擦测试过程中使用的摩擦副为直径 6 mm 的 SiO<sub>2</sub> 对偶球, 向模拟油气田 CO<sub>2</sub>-H<sub>2</sub>S-Cl<sup>-</sup>溶液中加入粒径为 1  $\mu\text{m}$  的 SiO<sub>2</sub> 粉末制成 SiO<sub>2</sub> 悬浊液, 在 3 种条件下对 4 种元素掺杂的 DLC 薄膜进行摩擦测试。第 1 种为

SiO<sub>2</sub> 对偶与薄膜在空气中的摩擦, 第 2 种为元素掺杂 DLC 薄膜在模拟油气田 CO<sub>2</sub>-H<sub>2</sub>S-Cl<sup>-</sup>溶液中的摩擦, 第 3 种为模拟油气田 CO<sub>2</sub>-H<sub>2</sub>S-Cl<sup>-</sup>悬浊液中的摩擦。摩擦测试的振幅和滑动频率分别为 2.5 mm 和 5 Hz, 循环次数为 20 000 转, 摩擦测试后的 SS304 基底与 DLC 薄膜通过 Archard 磨损公式计算磨损率。

2 结果及分析

2.1 元素掺杂 DLC 薄膜的微观结构

4 种不同元素掺杂 DLC 薄膜的拉曼光谱和截面形貌见图 1。所有元素掺杂的 DLC 薄膜在 1 000~1 700 cm<sup>-1</sup> 范围内均表现出一个宽的不对称峰<sup>[21-24]</sup>, 该特征峰可以被拟合为 D 峰和 G 峰。D 峰与芳香环和碳链中 sp<sup>2</sup>-C 原子的碳碳伸缩振动有关, G 峰对应于芳香环中 sp<sup>2</sup>-C 原子的对称呼吸振动。此外, I<sub>D</sub>/I<sub>G</sub> (D 峰与 G 峰的强度比)、G 峰的位置、FWHM<sub>G</sub> (G 峰的半峰宽) 分别与 DLC 薄膜的内应力水平、碳的无序程度和有序团簇的大小有关<sup>[25-27]</sup>。4 种元素掺杂 DLC 薄膜的 D 峰和 G 峰位置如表 2 所示, Si-HDLC 薄膜具有最低的 G 峰位置, 说明 Si-HDLC 薄膜具有最低的内应力; I<sub>D</sub>/I<sub>G</sub> 值间接反映了 DLC 薄膜中 sp<sup>3</sup>-C 杂化的含量, DLC 薄膜中 sp<sup>3</sup>-C 杂化的含量随 I<sub>D</sub>/I<sub>G</sub> 值的降低而增加<sup>[18,25]</sup>, 因此 Si-HDLC 薄膜具有最高的 sp<sup>3</sup>-C 含量和最小的 sp<sup>2</sup>-C 团簇尺寸。图 1e~h 为不同元素掺杂的 DLC 薄膜的截面形貌, 4 种 DLC 薄膜结构致密没有缺陷, 均与基底紧密结合。

2.2 元素掺杂 DLC 薄膜的力学性能

通过纳米压痕测试仪测试 4 种元素掺杂 DLC 薄膜的硬度 (H)、弹性模量 (E)、弹性系数 (H/E) 和塑性系数 (H<sup>3</sup>/E<sup>2</sup>) 见图 2。H-DLC 薄膜具有最高的硬度与弹性模量, 掺杂 F 和 N 后, DLC 薄膜的硬度降低, 这与 DLC 薄膜 sp<sup>3</sup>-C 含量的降低有关,

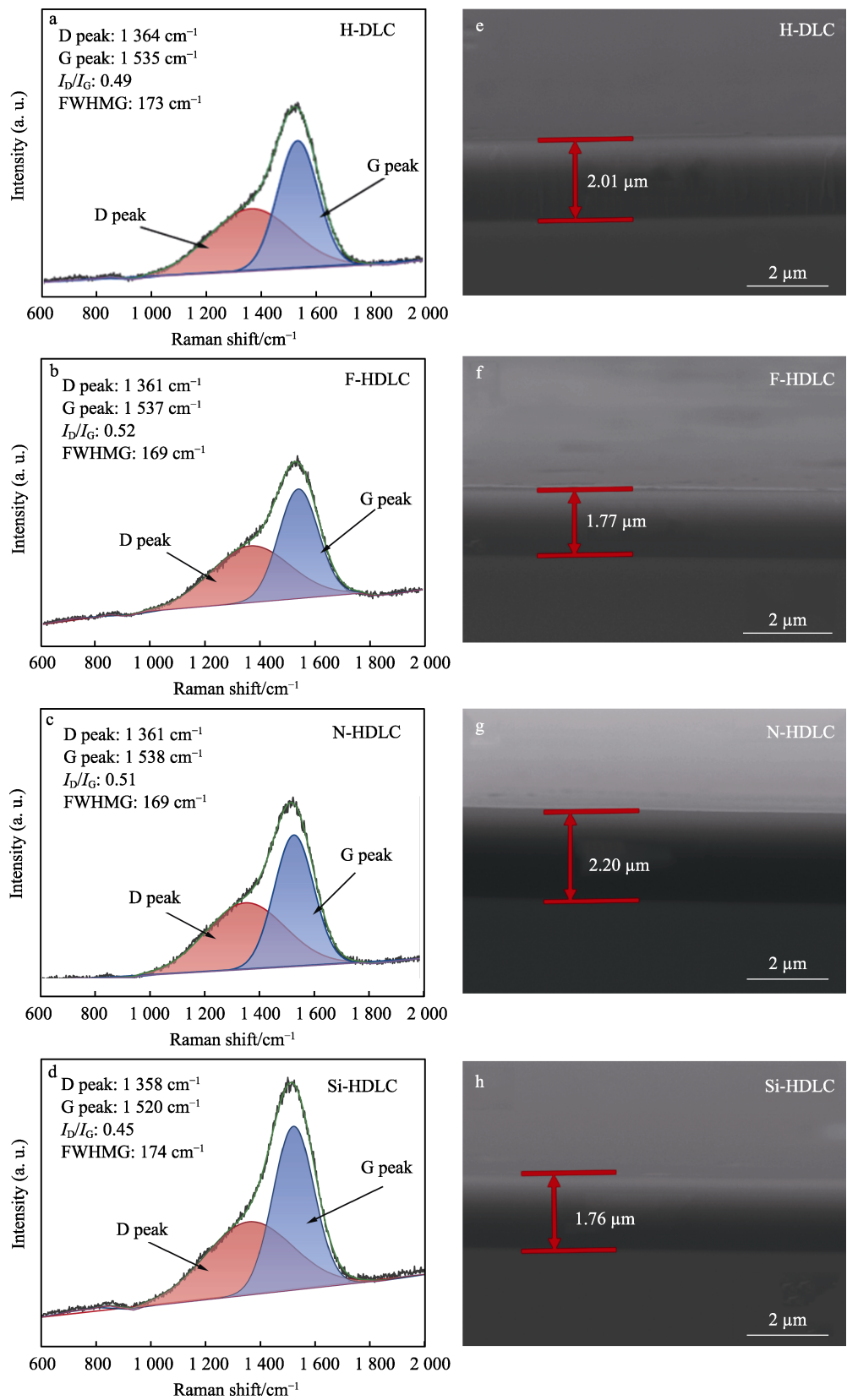


图 1 不同元素掺杂 DLC 薄膜的拉曼光谱 (a~d) 及截面形貌 (e~h)  
Fig.1 Raman spectra (a-d) and cross-sectional morphology (e-h) of DLC films doped with different elements

Si-HDLC 薄膜的  $I_D/I_G$  值最低, 具有最高的  $\text{sp}^3$  含量, 但其硬度值低于 H-DLC, 这归因于 Si-HDLC 薄膜的高含氢量。弹性系数是确定表面接触弹性行为极限的

有效方法之一, 塑性系数显示了材料对塑性变形的抵抗力, H-DLC 薄膜具有最高的弹性系数与塑性系数, 元素掺杂后 DLC 薄膜的弹性系数与塑性系数均降低,

但高于 SS304 基底 ( $H/E \approx 0.02$ ,  $H^3/E^2 \approx 0.002$  GPa), 与 SS304 基底相比, 4 种元素掺杂的 DLC 薄膜均具有优异的机械性能。4 种元素掺杂 DLC 薄膜的划痕形貌如图 3 所示,  $L_{c1}$  代表薄膜的起始剥落点,  $L_{c3}$  为薄膜的连续剥落点, 4 种元素掺杂 DLC 薄膜的  $L_{c1}$  值在 3.2~4.3 N 之间,  $L_{c3}$  值在 12.5~13.8 N 之间, Si 过渡层的沉积减少了基底和 Si-DLC 薄膜之间的失配, 大大提高了薄膜与基底间的结合力<sup>[28]</sup>, 4 种元素掺杂的 DLC 薄膜均具有良好的结合力, 避免了在腐蚀过程中因为膜基界面起泡而导致薄膜脱落<sup>[29]</sup>, Si 元素掺杂的 DLC 薄膜具有最高的  $L_{c1}$  值与  $L_{c3}$  值。

表 2 不同元素掺杂 DLC 薄膜拉曼光谱的 D 峰和 G 峰位置  
Tab.2 D peak and G peak positions of Raman spectra of DLC films doped with different elements

Films	D peak position/cm <sup>-1</sup>	G peak position/cm <sup>-1</sup>
H-DLC	1 364	1 535
F-HDLC	1 361	1 537
N-HDLC	1 361	1 538
Si-HDLC	1 358	1 520

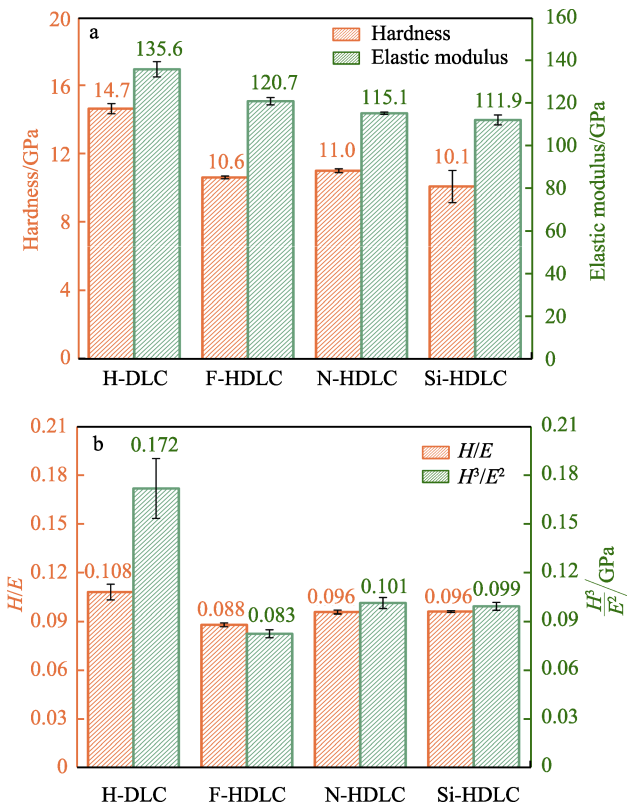


图 2 不同元素掺杂 DLC 薄膜的硬度和弹性模量 (a) 以及弹性系数与塑性系数 (b)  
Fig.2 Hardness and elastic modulus (a) and elastic coefficient and plastic coefficient (b) of DLC films doped with different elements

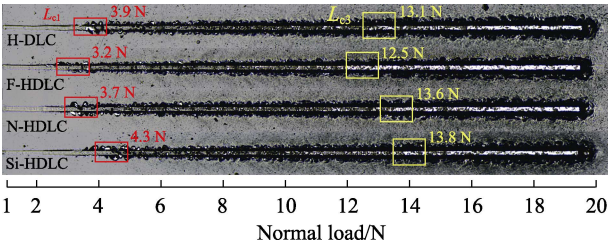


图 3 不同元素掺杂 DLC 薄膜的划痕形貌  
Fig.3 Scratch morphology of DLC films doped with different elements

2.3 元素掺杂 DLC 薄膜在模拟油气田溶液中的腐蚀行为

图 4 为 4 种元素掺杂 DLC 薄膜的动电位极化曲线和电化学阻抗谱曲线。元素掺杂 DLC 薄膜的腐蚀电位 ( $E_{corr}$ )、腐蚀电流密度 ( $J_{corr}$ ) 和极化电阻 ( $R_p$ ) 见表 3。DLC 薄膜的极化电阻通过公式 (1) 计算。

$$R_p = \frac{\beta_a \cdot \beta_c}{2.303 J_{corr} (\beta_a + \beta_c)} \tag{1}$$

式中:  $\beta_a$  和  $\beta_c$  分别代表了阳极和阴极的塔菲尔斜率,  $J_{corr}$  代表了基底和薄膜的腐蚀电流密度。

从图 4a 和表 3 中可以看出, Si-HDLC 薄膜具有最低的腐蚀电流密度和最高的极化电阻, F-HDLC 与 N-HDLC 薄膜的腐蚀电流密度略高于 H-DLC, 且 4 种不同元素掺杂的 DLC 薄膜的腐蚀电流密度均显著低于 SS304 基底。DLC 薄膜的沉积显著提高了 SS304 基底在模拟油气田环境中的耐蚀性。

图 4b~d 为不同元素掺杂 DLC 薄膜的电化学阻抗谱 (EIS)。图 4b 中的 Bode 图半圆环的半径反映了材料的耐蚀性, 半圆环半径越大, 薄膜的耐蚀性越高<sup>[28]</sup>。图 4d 中的 Nyquist 图低频处的阻抗值也能反映 DLC 薄膜的耐蚀性, 低频处的阻抗值越高, 材料的耐蚀性越好。Si-HDLC 薄膜具有最大的半圆环半径与最高的低频阻抗, 说明 Si-HDLC 薄膜具有最强的耐蚀性, 这与图 4a 动电位极化曲线中的耐蚀性结果一致。

为了更好地理解 SS304 基底和不同元素掺杂 DLC 薄膜的腐蚀行为, 使用图 4e~h 的等效电路对 SS304 基底及 4 种元素掺杂的 DLC 薄膜的电化学阻抗谱进行拟合, 图中  $R_s$  代表溶液电阻,  $R_c$  和  $CPE_c$  代表 DLC 薄膜的孔隙电阻及其相应的电容,  $R_{dl}$  和  $CPE_{ct}$  分别代表双电层电阻和电容,  $W_1$  为表征腐蚀产物的 Warburg 阻抗,  $R_{diff}$  和  $CPE_{diff}$  表示腐蚀产物扩散产生的扩散电阻及扩散电容。SS304 基底在图 4b 的 Nyquist 图中仅显示出一个电容环, 因此通过图 4e 中的等效电路拟合。F-HDLC、N-HDLC 和 Si-HDLC 薄膜在图 4c 的 Bode 图中能够观察到 3 个时间常数, 高频处的时间常数代表了腐蚀溶液从 DLC 薄膜表面向内渗透, 中频处的时间常数表明腐蚀溶液已经渗透到

了薄膜与基底界面形成双电层,低频处的时间常数说明腐蚀溶液与基底接触后形成了腐蚀产物并沿着薄膜的孔隙向外扩散<sup>[30]</sup>。Si-HDLC 薄膜的阻抗谱由图 4g 中的等效电路拟合。在图 4b 的 Nyquist 图中, F-HDLC 和 N-HDLC 薄膜代表扩散的曲线与 Si-HDLC 薄膜不同,表明这种扩散行为不再能通过 Warburg 阻抗来表示,由于涂层对腐蚀产物的扩散具有阻隔性能,扩散过程能够成为法拉第过程中的一个控制程序<sup>[31-34]</sup>,因此 F-HDLC 和 N-HDLC 薄膜的等效电路为图 4h。因为这一扩散过程通常发生在 Warburg 扩散之后,所以薄膜与基底界面产生了更多向外扩散的腐蚀产物,说明 Si-HDLC 薄膜具有比

F-HDLC 和 N-HDLC 薄膜更高的耐蚀性。H-DLC 薄膜在 Bode 图中仅观察到了 2 个时间常数,高频处代表溶液渗透的时间常数消失,这说明 H-DLC 薄膜对腐蚀溶液的渗透无法起到良好的阻隔作用,同时 H-DLC 薄膜在低频处代表扩散的时间常数由半无限层的扩散转变为了有限层的扩散,这意味着滞留层的厚度变为了有限值,说明薄膜与基底界面的反应剧烈,因此 H-DLC 薄膜比起其余 3 种元素掺杂的薄膜耐蚀性更差,表 4 总结了 SS304 基底和 4 种元素掺杂的 DLC 薄膜的等效电路参数。Si-HDLC 薄膜具有最高的孔隙电阻,在模拟油气田溶液中 Si-HDLC 薄膜能起到最好的阻隔作用,减缓腐蚀介质的渗透。

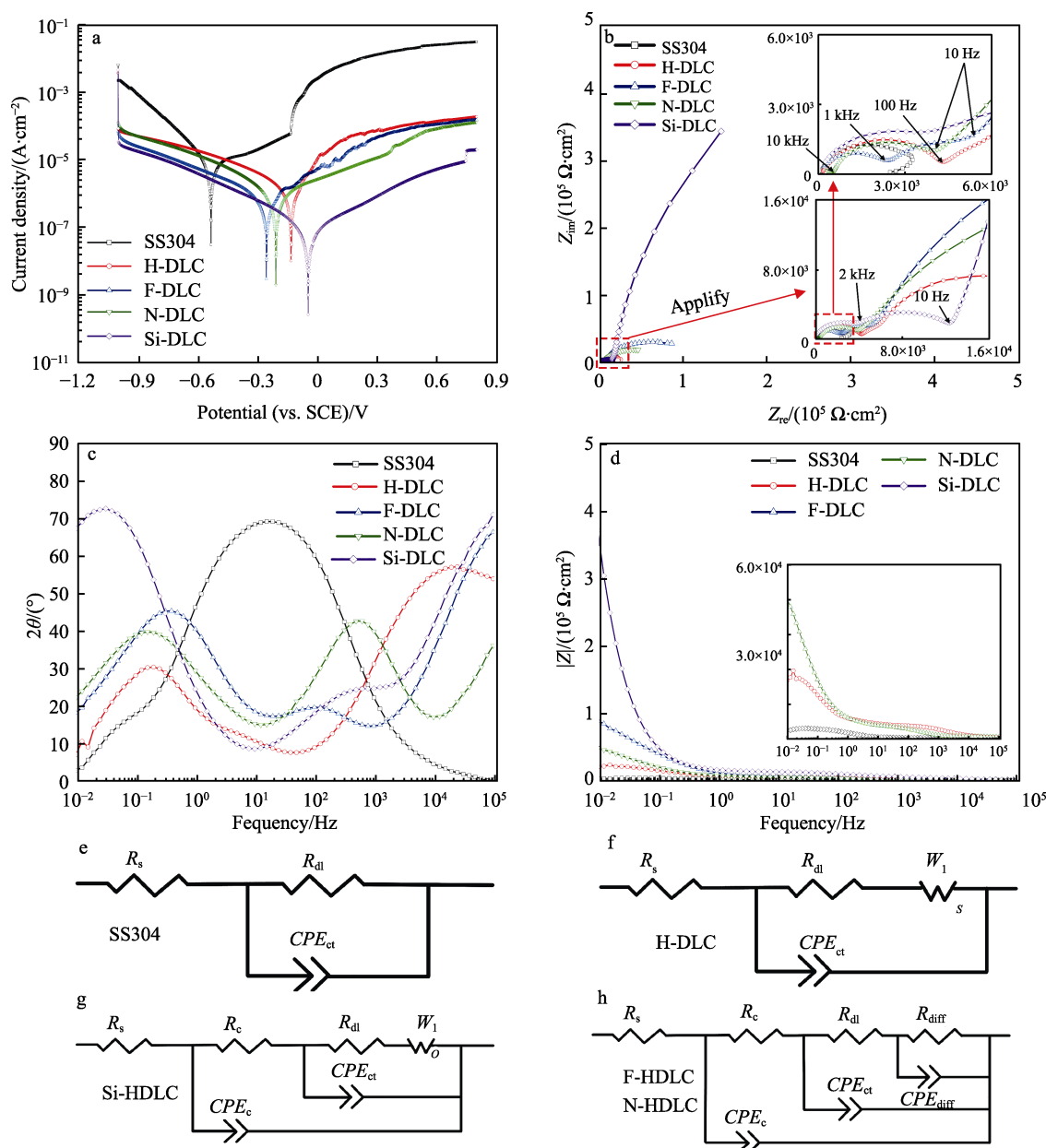


图 4 不同元素掺杂 DLC 薄膜与 SS304 在模拟油气田  $\text{CO}_2/\text{H}_2\text{S}/\text{Cl}^-$  溶液中的动电位极化曲线 (a)、电化学阻抗谱 (b~d) 和等效电路 (e~h)

Fig.4 Potentiodynamic polarization curves (a), electrochemical impedance spectroscopy (b-d) and equivalent circuit (e-h) of DLC films doped with different elements and SS304 in simulated oil and gas field  $\text{CO}_2/\text{H}_2\text{S}/\text{Cl}^-$  solution

表 3 SS304 和不同元素掺杂 DLC 薄膜通过 Tafel 极化曲线获得的  $E_{\text{corr}}$ 、 $J_{\text{corr}}$ 、 $\beta_c$ 、 $\beta_a$  和  $R_p$   
Tab.3  $E_{\text{corr}}$ ,  $J_{\text{corr}}$  and  $R_p$  of SS304 and DLC films doped with different elements obtained by Tafel polarization curves

Samples	$E_{\text{corr}}$ (vs. SCE)/V	$J_{\text{corr}}$ /(A·cm <sup>-2</sup> )	$\beta_c$ /V	$\beta_a$ /V	$R_p/\Omega$
SS304	-0.533	1.39×10 <sup>-5</sup>	0.199	0.782	4.96×10 <sup>3</sup>
HDLC	-0.131	1.37×10 <sup>-6</sup>	0.345	0.164	3.51×10 <sup>4</sup>
F-HDLC	-0.254	1.01×10 <sup>-6</sup>	0.442	0.285	7.43×10 <sup>4</sup>
N-HDLC	-0.208	1.19×10 <sup>-6</sup>	0.319	0.435	6.70×10 <sup>4</sup>
Si-HDLC	-0.045	1.38×10 <sup>-7</sup>	0.346	0.533	6.59×10 <sup>5</sup>

表 4 SS304 和不同元素掺杂 DLC 薄膜的等效电路参数  
Tab.4 Equivalent circuit parameters of SS304 and DLC films doped with different elements

Samples	$R_{\text{dl}}/(\text{10}^3 \Omega \cdot \text{cm}^2)$	$Y_{\text{ct}}/(\text{10}^{-7} \Omega^{-1} \cdot \text{cm}^{-2} \cdot \text{s}^n)$	$n_{\text{ct}}$	$R_{\text{c}}/(\Omega \cdot \text{cm}^2)$	$Y_{\text{c}}/(\text{10}^{-8} \Omega^{-1} \cdot \text{cm}^{-2} \cdot \text{s}^n)$	$n_{\text{c}}$	$\frac{W_{\text{R1}}}{R_{\text{diff}}} / (\text{10}^3 \Omega \cdot \text{cm}^2)$	$\frac{W_{\text{T1}}}{R_{\text{diff}}} / (\Omega^{-1} \cdot \text{cm}^{-2} \cdot \text{s}^n)$	$\frac{W_{\text{p}}}{n_{\text{diff}}}$	Chi-Square/ 10 <sup>-4</sup>
SS304	3.26	953	0.84							133
H-DLC	4.13	2.42	0.76				18.1	5.49	0.48	23.8
F-HDLC	6.82	156	0.52	2 260	4.16	0.81	106	1.43×10 <sup>-5</sup>	0.89	11.8
N-HDLC	3.41	6.22	0.89	773	43.4	0.61	63.4	6.67×10 <sup>-5</sup>	0.67	5.07
Si-HDLC	6.57	4.34	0.82	5 280	5.09	0.76	4.09	0.71	0.43	20.3

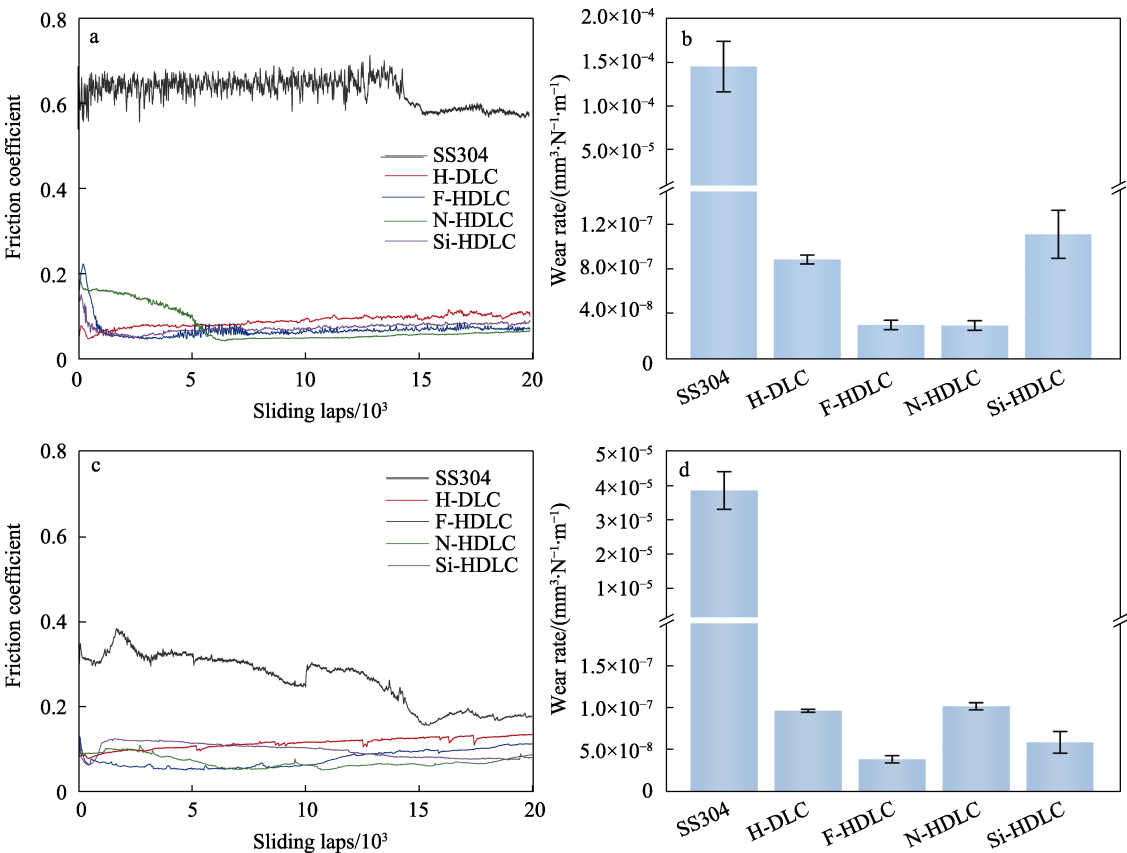


图 5 SS304 基底与不同元素掺杂 DLC 薄膜在空气 (a、b) 与模拟油气田  $\text{CO}_2/\text{H}_2\text{S}/\text{Cl}^-$  溶液 (c、d) 中的摩擦因数与磨损率  
Fig.5 Friction coefficient and wear rate of SS304 substrate and DLC films doped with different elements in air (a, b) and simulated oil and gas field  $\text{CO}_2/\text{H}_2\text{S}/\text{Cl}^-$  solution (c, d)

润滑作用下 SS304 基底的磨损率由在大气中的  $1.45 \times 10^{-4} \text{ mm}^3/(\text{N} \cdot \text{m})$  降低至  $3.81 \times 10^{-4} \text{ mm}^3/(\text{N} \cdot \text{m})$ , Si-HDLC 薄膜的磨损率由大气中的  $1.12 \times 10^{-4} \text{ mm}^3/(\text{N} \cdot \text{m})$  降低至溶液中的  $5.78 \times 10^{-4} \text{ mm}^3/(\text{N} \cdot \text{m})$ 。图 6a~d 为元素掺杂 DLC 薄膜在大气中进行摩擦测试后的磨斑形貌, 磨斑表面能观察到明显的物质沉积, 通过 EDS 元素成分分析可以发现该物质中含有 C 元素, 因此在磨损过程中存在转移膜的生成, 转移膜的形成大幅降低了 DLC 薄膜的磨损率<sup>[35]</sup>。图 6e~h 为元素掺杂 DLC 薄膜在模拟油气田溶液中摩擦测试后的磨斑形貌, 在腐蚀溶液中磨斑表面物质沉积数量减少, 通过 EDS 元素成分分析在磨斑表面仍能观察到 C 元素, 这意味着

在腐蚀溶液中仍然存在转移膜的生成。氯离子的离子半径很小, 在腐蚀过程中能够渗透至腐蚀产物与基底之间形成屏障来降低腐蚀产物的黏附<sup>[36-37]</sup>, 氯离子的屏障作用可能是转移膜减少的原因之一, DLC 薄膜在模拟油气田  $\text{CO}_2\text{-H}_2\text{S-Cl}^-$  溶液中具有优异的结构与成分稳定性, 薄膜不会因为腐蚀溶液而被破坏<sup>[20]</sup>, 在该溶液中仍能形成部分转移膜来降低摩擦因数与磨损率, 同时腐蚀溶液起到了润滑作用, 因此在模拟油气田  $\text{CO}_2\text{-H}_2\text{S-Cl}^-$  溶液中 DLC 薄膜均具有更低的磨损率。

用来模拟沙粒磨损的  $\text{SiO}_2$  形貌如图 7a 所示, 颗粒的直径约为  $1 \mu\text{m}$ 。图 7b 为 SS304 基底在含有  $\text{SiO}_2$

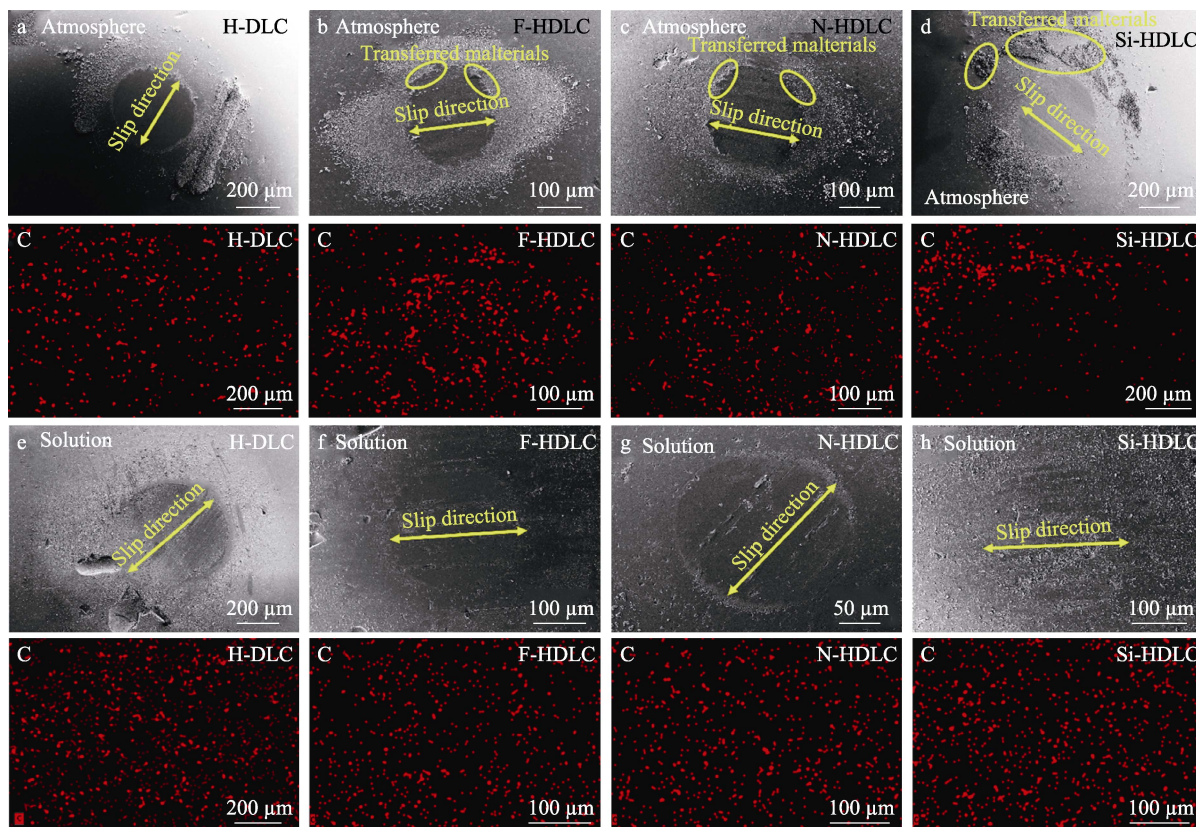


图 6 DLC 薄膜在大气 (a~d) 与模拟油气田  $\text{CO}_2/\text{H}_2\text{S}/\text{Cl}^-$  溶液 (e~h) 中的磨斑形貌

Fig.6 Wear scar morphology of DLC films in atmosphere (a-d) and simulated oil and gas fields  $\text{CO}_2/\text{H}_2\text{S}/\text{Cl}^-$  solution (e-h)

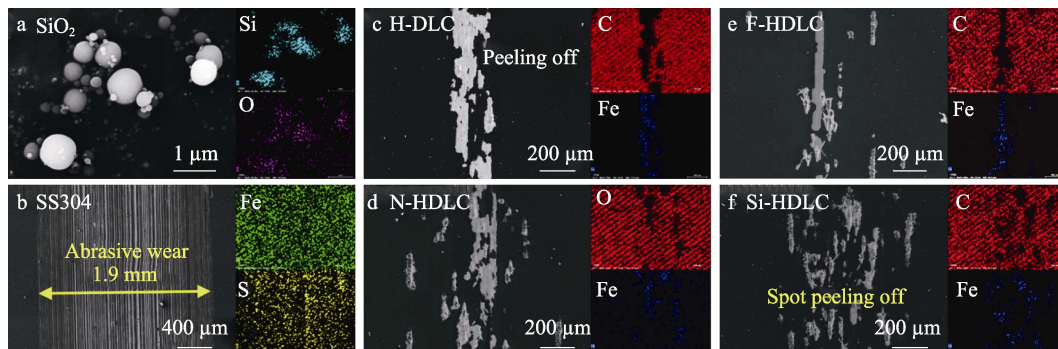


图 7  $\text{SiO}_2$  颗粒形貌 (a) 与 SS304 (b) 及不同元素掺杂 DLC 薄膜 (c~f) 在含有  $\text{SiO}_2$  颗粒的模拟油气田  $\text{CO}_2/\text{H}_2\text{S}/\text{Cl}^-$  溶液中的磨痕形貌

Fig.7 Morphology of  $\text{SiO}_2$  particles (a) and wear scar morphology of SS304 (b) and DLC films doped with different elements (c-f) in  $\text{CO}_2/\text{H}_2\text{S}/\text{Cl}^-$  solution of simulated oil and gas fields containing  $\text{SiO}_2$  particles

粉末的模拟油气田悬浊液中的磨痕形貌, 磨痕表面存在大量的犁沟,  $\text{SiO}_2$  颗粒的存在使基底表面发生磨粒磨损, 大幅增加了基底的磨损率。图 7c~f 为不同元素掺杂 DLC 薄膜在含有  $\text{SiO}_2$  颗粒的模拟油气田溶液中的磨痕形貌, H-DLC 薄膜磨痕表面发生大面积剥落, 元素掺杂后薄膜连续剥落的情况减少, DLC 薄膜由连续剥落转变为点状剥落, DLC 薄膜的沉积显著提高了 SS304 基底在含有  $\text{SiO}_2$  颗粒溶液中的耐磨性, 大大缓解了基底的磨粒磨损。

### 3 结论

1) 通过 PECVD 技术在 SS304 基底表面沉积了 H-DLC、F-HDLC、N-HDLC 和 Si-HDLC 4 种 DLC 薄膜, DLC 薄膜的沉积显著提高了 SS304 基底在模拟油气田  $\text{CO}_2/\text{H}_2\text{S}/\text{Cl}^-$  环境中的耐蚀性, 沉积薄膜后基底的  $J_{\text{corr}}$  值由  $1.39 \times 10^{-5} \text{ A/cm}^2$  降低至  $1.38 \times 10^{-7} \text{ A/cm}^2$ , DLC 薄膜的阻隔作用有效地减缓了基底的腐蚀速率。同时, DLC 薄膜的沉积显著降低了 SS304 基底在与模拟泥沙中  $\text{SiO}_2$  对偶间摩擦的磨损率, 薄膜的沉积使磨损率下降了约 2 个数量级。

2) DLC 薄膜在与模拟沙粒的  $\text{SiO}_2$  对偶球间的摩擦时能够形成稳定的转移膜, 大幅降低摩擦因数与磨损率, 同时不同元素掺杂的 DLC 薄膜在  $\text{CO}_2/\text{H}_2\text{S}/\text{Cl}^-$  溶液中仍能形成转移膜。

3) 向模拟油气田的  $\text{CO}_2/\text{H}_2\text{S}/\text{Cl}^-$  溶液中加入  $\text{SiO}_2$  颗粒后, SS304 基底的磨损率大幅提高, 磨痕表面发生严重的磨粒磨损, 然而 DLC 薄膜的沉积仍显著减缓了基底的磨损, 对油气开采管道的内表面具有良好的保护效果。

### 参考文献:

- [1] 鲁喜宁, 杨玘, 欧阳志英. 油井管螺纹的表面处理技术研究及进展[J]. 材料保护, 2023, 56(9): 154-160.  
LU X N, YANG P, OUYANG Z Y. Research and Development Progress of Surface Treatment Technology for Oil Well Pipe Thread[J]. Materials Protection, 2023, 56(9): 154-160.
- [2] WANG Z M, ZHANG J, HAN X, et al. Corrosion and Salt Scale Resistance of Multilayered Diamond-Like Carbon Film in  $\text{CO}_2$  Saturated Solutions[J]. Corrosion Science, 2014, 86: 261-267.
- [3] LEI X W, WANG H Y, MAO F X, et al. Electrochemical Behaviour of Martensitic Stainless Steel after Immersion in a  $\text{H}_2\text{S}$ -Saturated Solution[J]. Corrosion Science, 2018, 131: 164-173.
- [4] MOHTADI-BONAB M, SZPUNAR J, RAZAVI-TOUSI S. Hydrogen Induced Cracking Susceptibility in Different Layers of a Hot Rolled X70 Pipeline Steel[J]. International Journal of Hydrogen Energy, 2013, 38(31): 13831-13841.
- [5] SANTOS B A F, SOUZA R C, SERENARIO M E D, et al. The Effect of Different Brines and Temperatures on the Competitive Degradation Mechanisms of  $\text{CO}_2$  and  $\text{H}_2\text{S}$  in API X65 Carbon Steel[J]. Journal of Natural Gas Science and Engineering, 2020, 80: 103405.
- [6] SUN C, ZENG H B, LUO J L. Unraveling the Effects of  $\text{CO}_2$  and  $\text{H}_2\text{S}$  on the Corrosion Behavior of Electroless Ni-P Coating in  $\text{CO}_2/\text{H}_2\text{S}/\text{Cl}^-$  Environments at High Temperature and High Pressure[J]. Corrosion Science, 2019, 148: 317-330.
- [7] 黄强. 地面集输管道在  $\text{CO}_2/\text{H}_2\text{S}/\text{O}_2$  体系下的腐蚀行为研究[J]. 表面技术, 2021, 50(4): 351-360.  
HUANG Q. Research on Corrosion Behavior of Ground Gathering Pipeline under  $\text{CO}_2/\text{H}_2\text{S}/\text{O}_2$  System[J]. Surface Technology, 2021, 50(4): 351-360.
- [8] 李佳航, 王丹, 谢飞, 等. 油气管道的  $\text{CO}_2$  腐蚀及防护研究进展[J]. 表面技术, 2021, 50(4): 172-183.  
LI J H, WANG D, XIE F, et al. Research Progress on  $\text{CO}_2$  Corrosion and Protection of Oil and Gas Pipelines[J]. Surface Technology, 2021, 50(4): 172-183.
- [9] 沈哲, 康留香, 李丛妮. 陕北油田集输管线腐蚀原因分析及腐蚀防护技术研究[J]. 表面技术, 2021, 50(5): 253-260.  
SHEN Z, KANG L X, LI C N. The Corrosion Analysis and Research of Corrosion Protection Technology of Gathering and Transportation Pipeline in Shanbei Oilfield[J]. Surface Technology, 2021, 50(5): 253-260.
- [10] WEI X B, NING C M, LU Z B, et al. Si and N Incorporated Hydrogenated Diamond Like Carbon Film with Excellent Performance for Marine Corrosion Resistance[J]. Ceramics International, 2022, 48(6): 8440-8450.
- [11] ERDEMIR A, DONNET C. Tribology of Diamond-Like Carbon Films: Recent Progress and Future Prospects[J]. Journal of Physics D: Applied Physics, 2006, 39(18): R311-R327.
- [12] MA F, CAI X, LI G, et al. Characterization of the Diamond-Like Carbon Based Functionally Gradient Film[J]. Journal of Materials Science & Technology, 2002, 18(5): 447-450.
- [13] ROBERTSON J. Diamond-Like Amorphous Carbon[J]. Materials Science and Engineering: R: Reports, 2002, 37(4/5/6): 129-281.
- [14] XU X W, GUO P, ZUO X, et al. Understanding the Effect of Al/Ti Ratio on the Tribocorrosion Performance of Al/Ti Co-Doped Diamond-Like Carbon Films for Marine Applications[J]. Surface and Coatings Technology, 2020, 402: 126347.
- [15] LI X B, HOU K, QIU D K, et al. A First Principles and Experimental Study on the Influence of Nitrogen Doping on the Performance of Amorphous Carbon Films for Proton Exchange Membrane Fuel Cells[J]. Carbon, 2020, 167: 219-229.
- [16] WANG X Y, ZHOU H B, ZHANG S T, et al. The Effect

- of Acetylene Flow Rate on the Uniform Deposition of Thick DLC Coatings on the Inner Surface of Pipes with Different Draw Ratios[J]. *Vacuum*, 2022, 196: 110720.
- [17] WEI X B, CAO X Q, YIN P M, et al. Design of a Novel Superhydrophobic F&Si-DLC Film on the Internal Surface of 304SS Pipes[J]. *Diamond and Related Materials*, 2022, 123: 108852.
- [18] WEI X B, CHEN L, ZHANG M L, et al. Effect of Dopants (F, Si) Material on the Structure and Properties of Hydrogenated DLC Film by Plane Cathode PECVD[J]. *Diamond and Related Materials*, 2020, 110: 108102.
- [19] WEI X B, FENG H Y, LIU Z Y, et al. Insight into the Corrosion Behaviors and Mechanism of the Self-Healing Si/N-DLC Films in Oilfield Environment[J]. *Corrosion Science*, 2024, 231: 111989.
- [20] LIU Z Y, YIN P M, MOU C L, et al. Corrosion Behavior of Si-DLC Film in Simulant Solutions Containing  $\text{CO}_2\text{-H}_2\text{S-Cl}^-$ [J]. *Surface and Coatings Technology*, 2024, 478: 130455.
- [21] CASIRAGHI C, FERRARI A C, ROBERTSON J. Raman Spectroscopy of Hydrogenated Amorphous Carbons[J]. *Physical Review B*, 2005, 72(8): 085401.
- [22] CASIRAGHI C, PIAZZA F, FERRARI A C, et al. Bonding in Hydrogenated Diamond-Like Carbon by Raman Spectroscopy[J]. *Diamond and Related Materials*, 2005, 14(3/4/5/6/7): 1098-1102.
- [23] FERRARI A C, ROBERTSON J. Interpretation of Raman Spectra of Disordered and Amorphous Carbon[J]. *Physical Review B*, 2000, 61(20): 14095-14107.
- [24] FERRARI A C, ROBERTSON J. Resonant Raman Spectroscopy of Disordered, Amorphous, and Diamond-like Carbon[J]. *Physical Review B*, 2001, 64(7): 075414.
- [25] BOCIAGA D, SOBCZYK-GUZENDA A, SZYMANSKI W, et al. Mechanical Properties, Chemical Analysis and Evaluation of Antimicrobial Response of Si-DLC Coatings Fabricated on AISI 316 LVM Substrate by a Multi-Target DC-RF Magnetron Sputtering Method for Potential Biomedical Applications[J]. *Applied Surface Science*, 2017, 417: 23-33.
- [26] CASIRAGHI C, FERRARI A C, ROBERTSON J. Raman Spectroscopy of Hydrogenated Amorphous Carbons[J]. *Physical Review B*, 2005, 72(8): 085401.
- [27] WEI X B, SHI S M, NING C M, et al. Si-DLC Films Deposited by a Novel Method Equipped with a Co-Potential Auxiliary Cathode for Anti-Corrosion and Anti-Wear Application[J]. *Journal of Materials Science & Technology*, 2022, 109: 114-128.
- [28] LIU Z Y, YIN P M, WEI X B, et al. Simultaneous Deposition of DLC Film on the Internal Surface of Multiple Pipes[J]. *Diamond and Related Materials*, 2022, 127: 109187.
- [29] 张鉴清, F. Mansfeld. 交流阻抗法评价有机涂层[J]. *腐蚀科学与防护技术*, 1989, 1(3): 15-21.
- [29] ZHANG J Q, MANSFELD F. Evaluation of Organic Coatings by AC Impedance Method[J]. *Corrosion Science and Protection Technology*, 1989, 1(3): 15-21.
- [30] CUI M J, PU J B, LIANG J, et al. Corrosion and Tribocorrosion Performance of Multilayer Diamond-Like Carbon Film in NaCl Solution[J]. *RSC Advances*, 2015, 5(127): 104829-104840.
- [31] HU J M, ZHANG J Q, CAO C N. Determination of Water Uptake and Diffusion of  $\text{Cl}^-$  Ion in Epoxy Primer on Aluminum Alloys in NaCl Solution by Electrochemical Impedance Spectroscopy[J]. *Progress in Organic Coatings*, 2003, 46(4): 273-279.
- [32] ZHANG J T, HU J M, ZHANG J Q, et al. Studies of Water Transport Behavior and Impedance Models of Epoxy-Coated Metals in NaCl Solution by EIS[J]. *Progress in Organic Coatings*, 2004, 51(2): 145-151.
- [33] ZHANG J T, HU J M, ZHANG J Q, et al. Studies of Impedance Models and Water Transport Behaviors of Polypropylene Coated Metals in NaCl Solution[J]. *Progress in Organic Coatings*, 2004, 49(4): 293-301.
- [34] ZHU C F, XIE R, XUE J H, et al. Studies of the Impedance Models and Water Transport Behaviors of Cathodically Polarized Coating[J]. *Electrochimica Acta*, 2011, 56(16): 5828-5835.
- [35] CHEN L, WANG J J, SHANG L L, et al. Gas Phase Lubrication on Diamond-Like Carbon Film: Tribochemical Reactions under Isobutane Condition[J]. *Tribology International*, 2019, 133: 152-159.
- [36] WANG S L, ZHANG G, FU A Q, et al. The Corrosion and Tribological Behaviors of DLC Film in  $\text{CO}_2$  Saturated NaCl Solution with High  $\text{Cl}^-$  Concentration[J]. *Diamond and Related Materials*, 2024, 144: 111016.
- [37] ZHANG N Y, ZENG D Z, XIAO G Q, et al. Effect of  $\text{Cl}^-$  Accumulation on Corrosion Behavior of Steels in  $\text{H}_2\text{S}/\text{CO}_2$  Methyldiethanolamine (MDEA) Gas Sweetening Aqueous Solution[J]. *Journal of Natural Gas Science and Engineering*, 2016, 30: 444-454.